SIMULATION OF A REACTIVE GAS-LIQUID SYSTEM WITH QUADRATURE-BASED MOMENTS METHOD

Antonio BUFFO[1,2], Marco VANNI[1] and Daniele L. MARCHISIO[1*]

[1] Department of Applied Science and Technology, Institute of Chemical Engineering, Politecnico di Torino, Torino, ITALY

[2] Department of Biotechnology and Chemical Technology, Aalto University, Espoo, FINLAND
*Corresponding author, E-mail address: daniele.marchisio@polito.it

ABSTRACT

The description of the interaction between fluid dynamics and fast chemical reactions in gas-liquid systems is complicated by the fact that the gas phase is poly-dispersed, namely it is constituted by bubbles characterized by a distribution of velocity, size and composition values. Phase coupling can be successfully described only if the modeling approach acknowledges the existence of this distribution, whose evolution in space and time is governed by the so-called Generalized Population Balance Equation (GPBE). A computationally efficient approach for solving the GPBE is represented by the Quadrature-Based Moment Methods (QBMM), where the evolution of the entire bubble population is recovered by tracking some specific moments of the distribution. In the present work, one of these methods, the Conditional Quadrature Method of Moments (CQMOM) has been implemented in the OpenFOAM two-fluid solver `compressibleTwoPhaseEulerFoam`, to simulate a chemically reacting gas-liquid system. To reduce the computational time and increase stability, a second-order operator-splitting technique for the solution of the chemically reacting species was also implemented, allowing to solve the different processes involved with their own time-scale. This modeling approach is here validated by comparing predictions with experiments, for the chemical absorption of CO_2 in NaOH solution, performed in a rectangular bubble column.

NOMENCLATURE

d_{32}	Mean Sauter bubble diameter (m)
G	Rate of bubble growth (m/s)
h	Collisional term of GPBE ($1/m^3s$)
L	Bubble size (m)
k	Turbulent kinetic energy (m^2/s^2)
$M_{k,l}$	Generic moment of the NDF($m^k mol^l/m^3$)
n	Number density function ($1/m^4 mol$)
N	Number of nodes of quadrature (-)
t	Time (s)
$\boldsymbol{u}$	Gas/liquid velocity (m/s)
$\boldsymbol{x}$	Spatial coordinates (m)

Greek letters

α	Gas volume fraction (-)
ε	Turbulent energy dissipation (m/s^3)
ν	Kinematic viscosity (m^2/s)
ρ	Density (kg/m^3)
ϕ	Bubble composition (mol)
$\dot{\phi}$	Rate of mass transfer (mol/s)

INTRODUCTION

The simulation of reacting turbulent gas-liquid bubbly systems is complicated by the fact that the disperse phase, constituted by gas bubbles, is highly polydisperse, namely the bubbles are characterized by very different size, velocity and composition values. In addition the fate of these bubbles is closely linked to the evolution of the continuous liquid phase through the so-called phase-coupling (Buffo and Marchisio, 2014). A plethora of methods is available for the simulation of such systems, and among them the most suitable method for simulating large-scale systems is the so-called Euler-Euler method (EEM). This method was originally formulated through a volume-average procedure, but can also be derived by applying the moment method to the main governing equation of multiphase systems, namely the generalized population balance equation (GPBE), as explained by Marchisio and Fox (2013).

The final equations that have actually to be solved are the transport equations for some moments of the number density function (NDF) that defines the polydispersity of the system. These moment equations are "unclosed" and to overcome the closure problem the NDF is reconstructed by using a quadrature approximation. The methods based on this approach are called Quadrature-Based Moment Methods (QBMM). Different approaches have been developed and in this work the Conditional Quadrature Method of Moments (CQMOM) is used. The rationale for using this method is that, as shows in our previous work (Buffo et al., 2012; Buffo et al. 2013b), for reacting systems, especially when the chemical reaction is fast, the NDF has to account for two "internal coordinates": bubble size and composition.

Following our previous work on this topic, our CQMOM implementation in the openFOAM solver `compressibleTwoPhaseEulerFoam` (Buffo et al., 2013a) is used to simulate a reacting gas-liquid system, for which experimental data are available in the literature (Darmana et al., 2007). It is important to stress here that the model is fully predictive: all the model constants have been derived from theory and no fitting constants are

adjusted here to match experiments. The chemical system investigated is very simple: a rectangular bubble column is filled with a NaOH aqueous solution and nitrogen is fluxed. Then abruptly the gas feed is changed to carbon dioxide, which transfers to the liquid phase and reacts with NaOH. Experimental measurements concerning plume oscillation period, global gas-hold hold up, mean Satuer diameter of the bubbles, pH time evolution are compared with model predictions resulting is very good agreement.

GOVERNING EQUATIONS

As shown by Marchisio and Fox (2013) by applying specific moment transforms to the GPBE the governing equations of fluid motion of phase *k* are readily derived:

$$\frac{\partial}{\partial t}(\rho_k \alpha_k) + \nabla \cdot (\rho_k \alpha_k \boldsymbol{u}_k) = 0 \tag{1}$$

$$\frac{\partial}{\partial t}(\rho_k \alpha_k \boldsymbol{u}_k) + \nabla \cdot (\rho_k \alpha_k \boldsymbol{u}_k \boldsymbol{u}_k) = -\nabla \cdot (\alpha_k \boldsymbol{\tau}_k) - \alpha_k \nabla p + \alpha_k \rho_k \boldsymbol{g} + M_k \tag{2}$$

where $\boldsymbol{u}_k$ is the Reynolds-averaged velocity for phase *k*. The stress tensor $\boldsymbol{\tau}_k$ for phase *k* is expressed as:

$$\boldsymbol{\tau}_k = \mu_{\text{eff},k}\left((\nabla \boldsymbol{u}_k) + (\nabla \boldsymbol{u}_k)^T - \frac{2}{3}\boldsymbol{I}(\nabla \cdot \boldsymbol{u}_k)\right), \tag{3}$$

where $\mu_{\text{eff},k}$ is the effective viscosity of phase *k*: $\mu_{\text{eff},l} = \mu_l + \mu_{t,l}$, μ_l is the molecular viscosity of the liquid and $\mu_{t,l} = \rho_l C_\mu \frac{k^2}{\varepsilon}$, *k* is the turbulent kinetic energy of the liquid phase and ε is the energy dissipation rate of the liquid phase. Both are calculated from the corresponding transport equations:

$$\frac{\partial}{\partial t}(\alpha_l k) + \nabla \cdot (\alpha_l k \boldsymbol{u}_l) - \nabla \cdot \left(\alpha_l \frac{\mu_{t,l}}{\rho_l \sigma_k}\nabla k\right) = \alpha_l(G - \varepsilon) \tag{4}$$

$$\frac{\partial}{\partial t}(\alpha_l \varepsilon) + \nabla \cdot (\alpha_l \varepsilon \boldsymbol{u}_l) - \nabla \cdot \left(\alpha_l \frac{\mu_{t,l}}{\rho_l \sigma_\varepsilon}\nabla \varepsilon\right) = \alpha_l \left(C_{\varepsilon,1}\frac{\varepsilon}{k}G - C_{\varepsilon,2}\frac{\varepsilon^2}{k}\right) \tag{5}$$

with the model constants are those of the standard $k - \varepsilon$ model: $C_\mu = 0.09$, $\sigma_k = 1.0$, $\sigma_\varepsilon = 1.3$, $C_{\varepsilon,1} = 1.44$, and $C_{\varepsilon,2} = 1.92$. The term *G* is the turbulence production rate defined as: $G = 2\nu_{t,l}(\boldsymbol{S}:\nabla \boldsymbol{u}_l)$, where the strain rate tensor is in turn defined as $\boldsymbol{S} = \frac{1}{2}(\nabla \boldsymbol{u}_l + \nabla \boldsymbol{u}_l^T)$.

The term M_k in Eq. (2) describes coupling of the momentum balance equations that is derived based on a force balance acting on the bubbles in the liquid, defined by:

$$M_l = -M_g = M_{D,l} + M_{L,l} + M_{VM,l} \tag{6}$$

where forces on the right-hand side refer to drag, lift and virtual mass (of which in this work only the first is considered). The drag model considered in this work is based on the following expression:

$$C_D = (1 - \alpha_g)^{C_A} \max\left[\frac{24}{Re_{\text{eff}}}\left(1 + 0.15 Re_{\text{eff}}^{0.687}\right), \frac{8}{3}\frac{Eo}{Eo+4}\right]. \tag{7}$$

The effective Reynolds number is defined as follows:

$$Re_{\text{eff}} = \frac{\rho_l d_{32}|u_l - u_g|}{\mu_{\text{eff}}}, \text{ with } \mu_{\text{eff}} = \mu_l + C_B \rho_l \frac{k^2}{\varepsilon} \tag{8}$$

In Eq. (8) two corrections are applied to the standard drag force coefficient expression. The first one is related to the so-called crowding or swarm effect. When bubble are densely packed (i.e. $\alpha_k > 0.2$) their momentum boundary layers start interacting, resulting in non-linear effects on the drag force. The perceived drag force that each bubble "sees" is therefore higher that what predicted for a single isolated bubble, as witnessed by the larger gas hold-ups usually measured in "crowded" bubble columns. The second one is instead related to the so-called micro-scale turbulence, namely the turbulence on a length-scale smaller than the bubble size (that is therefore not resolved by the standard $k - \varepsilon$ model). Extensive comparison with experiments on a numerous apparatuses has allowed the identification of the two parameters as follows: $C_A = -1.3$ and $C_B = 0.002$.

As mentioned the bubble population is described through a NDF, so that the following quantity

$$n(L, \phi; \mathbf{x}, t)\mathrm{d}\phi \, \mathrm{d}L$$

represents the expected number of bubbles per unit volume with size ranging between *L* and *L*+d*L* and composition ranging between ϕ and ϕ+dϕ. In this work, an isothermal air-water system is investigated and composition is described by using the absolute number of moles of the chemical component contained in the bubble that transfer from one phase to another. In the test case investigated here, this chemical component is carbon dioxide, since nitrogen is assumed to be insoluble in the aqueous solution.

As well known the evolution of the NDF is dictated by the GPBE which reads as follows:

$$\frac{\partial n}{\partial t} + \nabla \cdot (\boldsymbol{u}_g \, n) + \frac{\partial}{\partial L}(G \, n) + \frac{\partial}{\partial \phi}(\dot\phi \, n) = h \tag{9}$$

where $\boldsymbol{u}_g$ is the bubble velocity, *G* represents the continuous rate of change of bubble size due to mass transfer, $\dot\phi$ is the continuous rate of change of bubble composition (i.e. moles of carbon dioxide) due to mass transfer and *h* is the term related to the discontinuous jump in bubble size and composition due to collisional events, such as coalescence and break up.

Sub-models containing the physics of such phenomena are needed to express these terms; the details can be found elsewhere (Buffo et al., 2013a). Here it is important to mention that all these sub-models are based on the local value of the turbulent dissipation rate, provided by the solution of the Eulerian two-fluid model. The mass transfer coefficient (and so the continuous change of bubble size) is estimated by means of the Danckwerts' penetration theory, in particular by considering the eddy renewal time equal to the Kolmogorov time-scale as prescribed by the Lamont and Scott (1970) model. In this work, turbulent fluctuations are considered as the only mechanism responsible for bubble coalescence and breakage; the coalescence efficiency is evaluated as the ratio between the contact and drainage time-scales, whereas bubble break up is assumed to result always in two bubbles with different sizes (prescribed by a β-PDF daughter distribution function) and equal compositions.

Recurring to the definition of the mixed order moment of the NDF:

$$M_{k,l}(\mathbf{x}, t) = \iint_0^{+\infty} n(L, \phi; \mathbf{x}, t)L^k \phi^l \, \mathrm{d}L \, \mathrm{d}\phi \tag{10}$$

It is possible to rewrite the GPBE in terms of mixed order moments as follows:

$$\frac{\partial M_{k,l}}{\partial t} + \nabla \cdot \left(\boldsymbol{u}_{k,l} M_{k,l} \right) + \int_0^{+\infty} k\, L^k (G\, n)\, \mathrm{d}L + \int_0^{+\infty} l\, \phi^l \left(\dot\phi\, n \right) \mathrm{d}\phi = h_{k,l} \quad (11)$$

where the velocity associated to the generic moment $\boldsymbol{u}_{k,l}$ and the collisional term $h_{k,l}$ are defined below:

$$\boldsymbol{u}_{k,l} = \frac{\iint_0^{+\infty} \boldsymbol{u}_g n\, L^k \phi^l \mathrm{d}L\, \mathrm{d}\phi}{M_{k,l}} \quad (12)$$

$$h_{k,l} = \iint_0^{+\infty} h\, L^k \phi^l\, \mathrm{d}L\, \mathrm{d}\phi \quad (13)$$

Since the collisional term is a complex functional of the NDF, there is a closure problem in the derived transport equations for the moments. By applying the so-called quadrature approximation (McGraw, 1997), the following functional assumption for the NDF is implicitly used:

$$n(L,\phi) = \sum_{i_1=1}^{N_1} \sum_{i_2=1}^{N_2} w_{i_1} w_{i_1,i_2}\, \delta\big[L - L_{i_1}\big] \delta\big[\phi - \phi_{i_1,i_2}\big]$$

where the N_1 weights w_{i_1}, the $N = N_1 N_2$ conditional weights w_{i_1,i_2} and the N nodes of quadrature $[L_{i_1}; \phi_{i_1,i_2}]$ are calculated from a specific set of mixed order moments with an efficient inversion algorithm. As it is possible to notice N_1 is the number of nodes used for size and N_2 for the composition conditioned over the i_1-th value of size. More details on this method can be found in the work of Yuan and Fox (2011).

An illuminating example is represented by the case with N_1=3 and N_2=1: six pure moments with respect to size are needed to calculate the three weights w_1, w_2 and w_3 and the three nodes L_1, L_2 and L_3 (i.e., $M_{0,0}$, $M_{1,0}$, $M_{2,0}$, $M_{3,0}$, $M_{4,0}$, $M_{5,0}$), then another three mixed-order moments are needed to calculate the three conditional weights $w_{1,1}$, $w_{2,1}$ and $w_{3,1}$ and conditional nodes $\phi_{1,1}$, $\phi_{2,1}$ and $\phi_{3,1}$ (i.e., $M_{0,1}$, $M_{1,1}$, $M_{2,1}$). The moment set employed with this solution contains the most important global properties of the gas-liquid system. For example the global gas volume fraction can be calculated from $M_{3,0}$ whereas the mean Sauter diameter d_{32} can be calculated as the ratio between $M_{3,0}$ and $M_{2,0}$. A detailed description of the algorithm and its application to gas-liquid systems can be found in the work of Buffo et al. (2013a,b) and we report here a very short summary. At each time step, the transport equations for the moments are solved, and the mean Sauter diameter is therefore determined. This value is in turn used to solve the momentum balance equations for the disperse and continuous phases. Then volume fractions for both phases are calculated and the loop is closed by moving on to the next time step.

TEST CASE, OPERATING CONDITIONS AND NUMERICAL DETAILS

In the test case simulated in this work a simple chemical reaction is experimentally investigated in the rectangular bubble column reported in Fig. 1. The column has a width of 200 mm, depth of 30 mm and height of 1500 mm. The front, back and both side walls are made of 10 mm thick glass plates, while the top and bottom part are made of stainless steel. During the experiment the column is filled with liquid up to a level of 1000 mm. The continuous liquid phase is an aqueous solution of NaOH containing therefore hydroxyl ions, whereas the disperse gaseous phase is carbon dioxide.
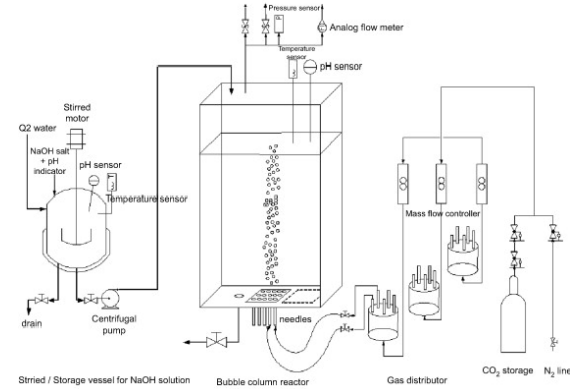

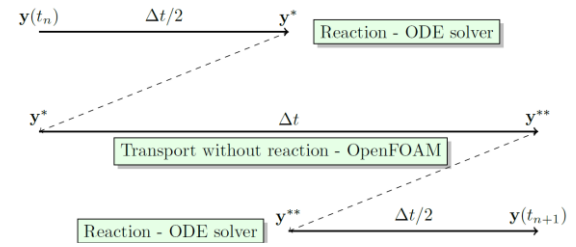
Figure 1: Sketch of the experimental set-up.

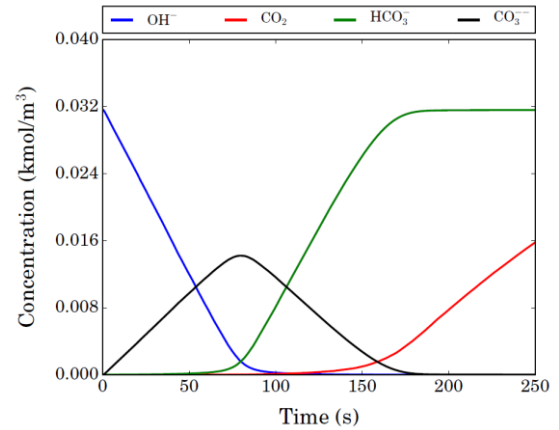**Figure 2**: Schematic representation of the operator-splitting approach.

Figure 3: Time evolution of the chemical species involved in the reaction resulting from the numerical simulation.

Experiments are performed by employing the following protocol. The column is first filled with an aqueous solution containing hydroxyl ions, nitrogen is introduced until the flow pattern is fully developed and then carbon dioxide in the form of gas bubbles is introduced in the bottom of the column (with a prescribed NDF exhibiting a log-normal size dependency), and the following reactions take place, while carbon dioxide is transferring from the gas to the liquid:

$$CO_{2(g)} \rightarrow CO_{2(aq)}$$
$$CO_{2(aq)} + OH^- \rightleftarrows HCO_3^-$$

$$HCO_3^- + OH^- \rightleftarrows CO_3^=$$
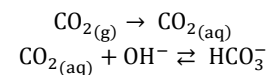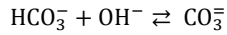
During experiments the pH is monitored and its time evolution is used for validation.

Numerical simulations of fast chemical reactions may be computationally demanding due to the small time step usually required to solve such problems.
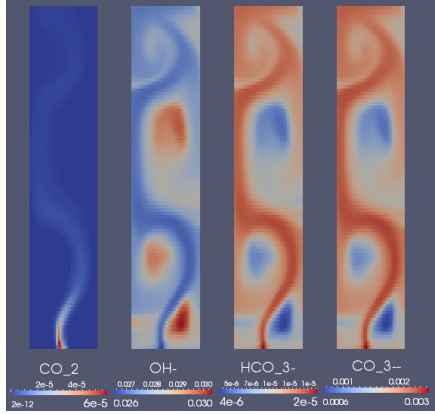

Figure 4: Instantaneous contour plots of the chemical species involved in the reaction after 10 s. From left to right dissolved CO_2, OH^-, HCO_3^-, $CO_3^=$.
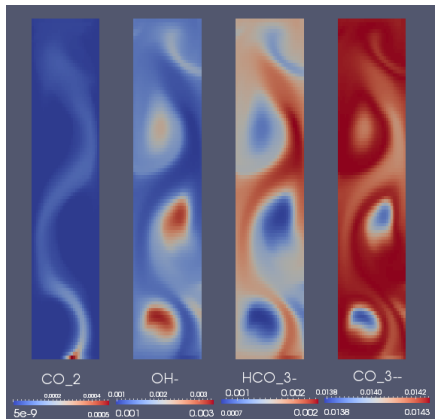

Figure 5: Instantaneous contour plots of the chemical species involved in the reaction after 80 s. From left to right dissolved CO_2, OH^-, HCO_3^-, $CO_3^=$.
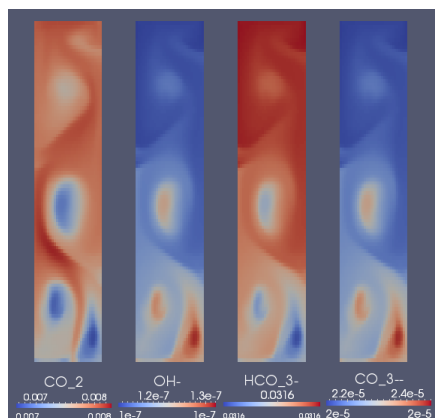

Figure 6: Instantaneous contour plots of the chemical species involved in the reaction after 200 s. From left to right dissolved CO_2, OH^-, HCO_3^-, $CO_3^=$.

To speed up the simulations it is often convenient to decouple the fast reaction kinetics from the fluid dynamics, through the use of an operator splitting approach. With this method, it is possible to integrate in time the different terms of a transport equation, each one with the proper numerical scheme; i.e., the reaction source term can be solved by means of a high-order ODE integrator specific for stiff/non-stiff problems, while the other terms can be solved with the standard first-order Backward Euler scheme. This method is capable of increasing the simulation stability and reducing the computational costs, since a larger time step can be used. For the present test case, a second order accurate operator splitting method, the so-called Strang Operator Spitting, has been implemented in openFOAM and used in all the simulations. A schematic representation of the algorithm is reported in Fig. 2.

It is important to mention that the expressions used in this work to estimate the reaction kinetics and the enhancement factor E are the same used in the work of (Darmana et al., 2007) and are here not reported for the sake of brevity. Figure 3 reports a typical example of the specie concentration time evolution predicted by this kinetic model: as carbon dioxide transfer to the liquid it is consumed by the first chemical reaction. When the concentration of hydroxyl ions becomes very low, the concentration of the bicarbonate ion starts increasing, and only when the second reaction reaches equilibrium the carbon dioxide concentration in solution starts increasing. For further details, readers may refer to this work.

As mentioned, the numerical simulations were carried out as follows: preliminary an inert gas is fluxed into the column filled with a NaOH solution with an initial pH of 12.5 until $t = 30$ s, in order to have the same initial condition of the reacting experiment, in which the fluid flow was developed through the flow of pure nitrogen. After this initial time interval, pure CO_2 is fed through the gas sparger at a superficial velocity of 7.7 mm/s (i.e. 2.2 ml/s per needle) and the calculation of the reaction kinetics is activated: through the mass transfer mechanism, some of the CO_2 contained in the gas bubbles will move to the liquid with the consequent start of the reversible two-step reactions reported above.

The final mesh employed in the simulations was constituted by 62×19×128 cells in the three directions. For the small section at the bottom where the gas entered the inlet boundary condition was used, whereas at the top the outflow boundary condition was used. All the other surface were described as walls (with no-slip condition).

RESULTS AND DISCUSSION

The evolution of the volume-average species concentrations during the reaction calculated by our model is depicted in Fig. 3, whereas Fig. 4 to 6 show contour plots at different time steps of the chemical species involved. As it is clear from the picture, all the dissolved CO_2 immediately reacts with hydroxide ions (OH^-) in the beginning of the process and it is directly converted into carbonate ($CO_3^=$). This means that in this phase the bicarbonate ion (HCO_3^-) concentration is almost equal to zero in all the domain, as Fig. 4 shows. Then, approximately after 80 s from the start of the reaction, the carbonate concentration reaches a maximum and then decreases; simultaneously, the bicarbonate concentration starts to increase. This situation can be observed also in Fig. 5, where the instantaneous contour plots for the chemical species involved in the reaction are represented. After about 190 s from the beginning of the reaction

experiment, the concentration of the bicarbonate ions reaches the initial OH^- concentration while $CO_3^=$ goes to zero almost everywhere in the reactor. At this point, the chemical reaction rates diminish and the dissolved CO_2 starts to accumulate in the liquid in the entire column, as it is possible to see in Fig. 6.

This behavior can be also seen in Fig. 7, where the experimental time evolution of pH in one point of the domain is compared with the numerical prediction. After 80 s we observe a change in the curve slope, which is caused by the shift of equilibrium of the second reaction (around pH 11) in favor of bicarbonate. Another change in pH slope is observed at about 190 s, when the first reaction is shifted towards dissolved CO_2, at pH approximately of 7.5. Through the comparison between experiment and simulation shown in Fig. 7 it is possible to conclude that the model is able to properly predict the time evolution of the reactions. From the qualitative point of view, the predicted pH curve shows a similar trend, with the change in the slope as observed in the experiment. From the quantitative point of view instead, it is possible to notice that the two curves are overlapped in the first 60 s, as also the comparison between simulation and experiment for the OH^- concentration reported in Fig. 8 shows. However, after 60 s the predicted pH evolution is slightly lagging behind compared to the experimental one; possible reasons of such disagreement can be the description of the second reaction, which is modeled with a finite rate through a high kinetic constant, instead of being considered instantaneous.
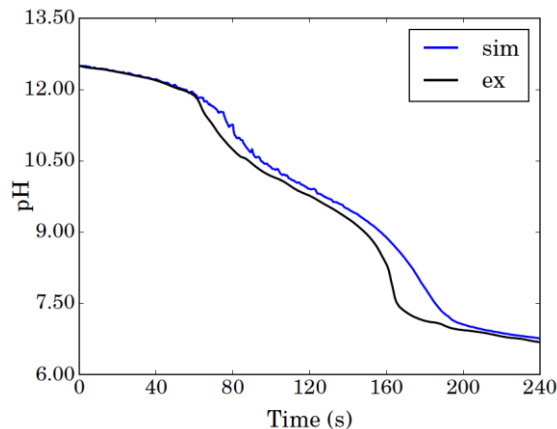

Figure 7: Comparison between predicted and experimental pH evolution in one point of the domain, located at $x = 0.1$ m, $y = 0.15$ m and $z = 0.95$ m.
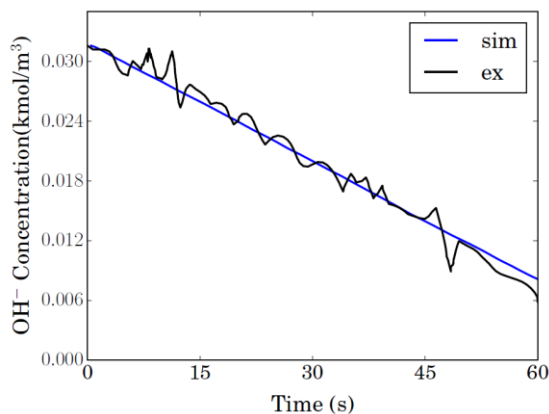

Figure 8: Comparison between predicted and experimental time evolution of OH^- concentration during the first 60 s of the reaction in one point of the domain, located at $x = 0.1$ m, $y = 0.15$ m and $z = 0.95$ m.

Table 1 shows further comparison with the experimental data, in terms of some fluid dynamics quantities such as global gas hold-up and plume oscillating period (POP). The global gas hold-up is simply calculated by averaging, in the region occupied by the liquid, the gas volume fraction. The POP is instead calculated by operating the Fourier transform of the pressure signal in one point of the geometry. As it is possible to notice, there is good agreement for such quantities, showing how this methodology is capable of properly predicting the fluid dynamic behavior of bubble columns in the homogeneous regime.

		Exp.	*Sim.*
Gas hold-up	*No-reaction*	2.3%	1.8%
	Reaction	1.3%	0.9%
POP	*No-reaction*	5.8 s	7.5 s
	Reaction	10.2 s	9.1 s

Table 1: Comparison of experimental data and prediction from the simulations for the global gas hold-up and plume oscillation period (POP).
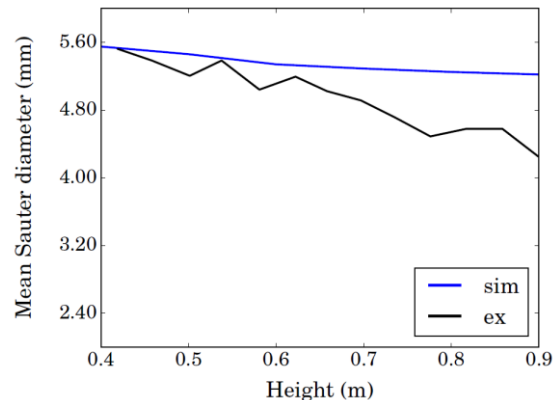

Figure 9: Comparison between prediction and experimental measurement for the mean Sauter diameter d_{32} (mm) at different heights of the column.

Figure 9 shows the comparison between simulation and experiment for the mean Sauter diameter, measured at different heights of the column. The predicted d_{32} line is composed by the time-average values from different points belonging to a line that connects two points: the central point at the top and at bottom of the column. As it is clear from the picture, the experimental trend is reproduced by the simulation, with the mean bubble diameter decreasing with the distance from the gas distributor. However, the present model seems to over-predict the bubble size: this is in contradiction with other comparisons shown before, as the one for the OH^- concentration in the early stages of the reaction, which proves that the mass transfer rate of CO_2 is properly predicted by the model. It is worth mentioning that the bubble diameter varies not only from point to point in the column, but also with time during the reaction: a precious information about the time interval at which the visual bubble diameter measurements have been performed is not reported in the experimental work. In addition, also the exact position of the camera is not

known, as well as the total number of bubbles per measurement point: this information is crucial for a detailed validation. In the absence of these, we can conclude that also this comparison is satisfactory.

CONCLUSION

In this work our own CQMOM implementation in the openFOAM solver `compressibleTwoPhaseEulerFoam` has been used to simulate a reacting gas liquid system. Since the reacting system involves a fast chemical reaction, as shown in our previous work, polydispersity with respect to both bubble size and composition, must be accounted for.

Simulation predictions, obtained with a fully predicted model with no adjustable modelling parameters, are compared with experiments, resulting in very good agreement. The model seems to be able to correctly predict the fluid dynamics of the bubble column, the evolution of the bubble size and the mass transfer rate between gas and liquid.

Future steps of this work include the extension of this methodology to the simulation of liquid-liquid dispersions, the development of reliable methodologies for dealing with poly-celerity (i.e. bubble gas velocity dependant on bubble size resulting in different moment velocities) and the development of more reliable kernels for coalescence and breakage.

ACKNOWLEDGEMENTS

REFERENCES

BUFFO, A. and MARCHISIO, D.L., (2014), "Modeling and simulation of turbulent polydisperse gas-liquid systems via the generalized population balance equation", *Reviews in Chemical Engineering*, **30**, 73-126.

BUFFO, A., MARCHISIO, D.L., and VANNI, M., (2012), "Multidimensional population balance model for the simulation of turbulent gas-liquid systems in stirred tank reactors", *Chemical Engineering Science*, **74**, 31-44.

BUFFO, A., MARCHISIO, D.L., VANNI, M. and RENZE, P. (2013a), "Simulation of polydisperse multiphase systems using population balances and example application to bubbly flows", *Chemical Engineering Research and Design*, **91**, 1859-1875.

BUFFO, A., VANNI, M., MARCHISIO, D.L., and FOX, R., (2013b), "Multivariate quadrature-based moments methods for turbulent polydisperse gas-liquid systems", *International Journal of Multiphase Flow*, **50**, 41-57.

DARMANA, D., HENKET, R., DEEN, N. and KUIPERS, J., (2007), "Detailed modelling of Hydrodynamics, mass transfer and chemical reactions in a bubble column using a discrete bubble model: Chemisorption of CO_2 into NaOH solution, numerical and experimental study", *Chemical Engineering Science*, **62**, 2556-2575.

LAMONT, J. C. and SCOTT, D. S., (1970), "An eddy cell model of mass transfer into the surface of a turbulent liquid", *AIChE Journal*, **16**, 513-519.

MARCHISIO, D.L. and FOX, R.O., (2013), *Computational Models for Polydisperse Particulate and Multiphase Systems*, Cambridge: Cambridge University Press.

MCGRAW, R., (1997), "Description of aerosol dynamics by the quadrature method of moments", *Aerosol Science and Technology*, **27**, 255-265.

YUAN, C. and Fox, R.O., (2011) "Conditional quadrature method of moments for kinetic equations," *Journal of Computational Physics*, **230**, 8216-8246.